

One-Shot Parameter Identification of the Thevenin's Model for Batteries: Methods and Validation[☆]

Ning Tian^a, Yebin Wang^b, Jian Chen^c, Huazhen Fang^{a,*}

^a*Department of Mechanical Engineering, University of Kansas, Lawrence, KS 66045, USA*

^b*Mitsubishi Electric Research Laboratories, Cambridge, MA 02139, USA*

^c*State Key Laboratory of Industrial Control Technology, College of Control Science & Engineering, Zhejiang University, Hangzhou 310027, China*

Abstract

Parameter estimation is of foundational importance for various model-based battery management tasks, including charging control, state-of-charge estimation and aging assessment. However, it remains a challenging issue as the existing methods generally depend on cumbersome and time-consuming procedures to extract battery parameters from data. Departing from the literature, this paper sets the unique aim of identifying all the parameters offline in a one-shot procedure, including the resistance and capacitance parameters and the parameters in the parameterized function mapping from the state-of-charge to the open-circuit voltage. Considering the well-known Thevenin's battery model, the study begins with the parameter identifiability analysis, showing that all the parameters are locally identifiable. Then, it formulates the parameter identification problem in a prediction-error-minimization framework. As the non-convexity intrinsic to the problem may lead to physically meaningless estimates, two methods are developed to overcome this issue. The first one is to constrain the parameter search within a reasonable space by setting parameter bounds, and the other adopts regularization of the cost function using prior parameter guess. The proposed identifiability analysis and identification methods are extensively validated through simulations and experiments.

Keywords: Battery, system identification, equivalent circuit model, Thevenin's model, nonlinear least squares, constrained optimization, regularization.

1. Introduction

Rechargeable batteries have found wide use nowadays in the consumer electronics, transportation and grid sectors by the billions. Their ever-widening use has excited an intense interest in advanced battery management system research. The main subjects of inquiry in this area include state-of-charge (SoC) and state-of-health (SoH) estimation, optimal charging control, cell balancing, thermal management, e.g., [1–12], and the references therein. Playing a foundational role in many of the existing studies are the equivalent circuit models (ECMs), which replicate a battery's electrical dynamics using a circuit composed of resistors, capacitors and voltage sources. However, the parameters

[☆]This work was supported in part by the United States National Science Foundation under Awards CMMI-1763093 and CMMI-1847651.

*Corresponding author. E-mail address: fang@ku.edu.

of an ECM are often unknown in many real-world circumstances or drift with cycled charging/discharging. This presents the question of how to accurately and efficiently identify them from the current/voltage measurements made on a battery cell.

The current literature on ECM identification can be roughly divided into three categories:

- **Experiment-based analysis.** This category develops and conducts charging/discharging experiments such that a battery's dynamics can be exposed and used to estimate parameters. For instance, the transient voltage responses are leveraged in [13, 14] to identify the internal resistance and RC-based time constants by charging or discharging a battery using constant or pulse currents. Another example is the experimental determination of the relationship between SoC and open-circuit voltage (OCV). Conventionally, it can be accomplished by charging or discharging the battery using a very small current [15–17], or alternatively, applying a current of normal magnitude intermittently (a sufficiently long rest period is applied between two discharging operations) [18–20]. While easy to implement, these approaches introduce significant time costs—an SoC-OCV calibration experiment can take more than one day [13, 15], unaffordable especially in massive battery testing. One can also find studies about the design of specialized charging/discharging protocols to expedite parameter identification, e.g. [21], which, however, would still take more than ten hours.
- **Electrochemical impedance spectroscopy (EIS).** EIS is an important means of observing electrochemical processes within batteries. The EIS data reveal the impedance properties of a battery, and the literature includes a few methods that fit an ECM to collected EIS data to extract the resistance and RC parameters [22–25]. These methods focus on impedance identification as needed in many applications and meanwhile, leave other parts of a battery's dynamics such as the SoC-OCV function beyond consideration.
- **Analytical data-based parameter estimation.** This category seeks to determine an ECM's unknown parameters using the current/voltage measurement data from a system identification perspective. The studies in [26–33] consider pulse current charging/discharging experiments and use the data to identify an ECM's RC parameters by fitting the model to the pulse phase voltage [26, 27], the relaxation phase voltage [28–31], or both of them [32, 33]. Some other studies perform similar data-fitting-based RC parameter estimation using data from variable current charging/discharging tests, while exploiting generic optimization [34], grey-box optimization [35], sequential quadratic programming [36], or particle swarm optimization [37, 38] as the solution tools. The studies in [39–42] propose to estimate the RC parameters by converting the identification problem into a problem of solving a set of linear and polynomial equations. In [43, 44], a linear state-space model is formulated for batteries, and subspace identification is then performed to infer the system matrices. An approach presented in [45] directly identifies the parameters of a continuous-time ECM using sampled discrete-time measurements. Associated with parameter identification, there is a growing amount of work on combined estimation of SoC and part of the model parameters [46–55]. It is noted that these studies usually require

an accurate SoC-OCV relationship to be available prior to identification, which requires long-time testing as aforementioned.

Despite the importance, the methods surveyed above, however, share one limitation: they are designed to identify only a subset of an ECM's parameters, on the premise that the other parameters are known. This brings about an intriguing question: *Is it possible to extract the parameters of an ECM all at once?* Here, by "all", it means the RC parameters as well as the parameters of the nonlinear SoC-OCV function. At least two benefits can result if this can be achieved. First, it will enhance the efficiency of battery model identification considerably by avoiding the tedious SoC-OCV calibration. Second, it can help ensure the availability of an accurate model for battery management during a battery's service life. However, one-shot identification for batteries has been long known as a challenge, because of the increase in the number of parameters to estimate and the serious nonlinearity and non-convexity in the identification procedure. The only studies on this topic, to our knowledge, are given in [56–59], which use the genetic algorithms to search for the best parameter estimates for a battery model. However, their application still face some limitations. The primary one among them is the weak parameter identifiability due to the many parameters (more than 30) to determine, which can potentially compromise the estimation accuracy. In addition, the genetic algorithms generally converge slowly and impose high computational expenses.

This work is motivated to develop new and efficient approaches for one-shot battery parameter identification. The Thevenin's model, which has been a popular choice for battery management [60–63], is considered here. This model is nonlinear by nature, and consequently, an identification effort can suffer pitfalls caused by the nonlinearity and non-convexity, which may eventually produce inaccurate or unphysical parameter estimation. This work hence presents a systematic study to overcome such an issue, yielding the following contributions.

- The study for the first time reveals the feasibility of the one-shot identification for the Thevenin's model through an in-depth parameter identifiability analysis. Specifically, it shows that all the parameters are locally identifiable, indicating that they can be uniquely determined in a local domain.
- With the model's local identifiability guaranteed, this work synthesizes novel one-shot parameter identification methods. The methods are developed to minimize the model prediction error through numerical optimization. Different from the literature, we introduce two critical mechanisms to address the non-convexity issue: 1) constrained optimization, which constrains the search space by applying upper and lower bounds to some parameters, and 2) generalized Tikhonov regularization, which adds a regularization term to the considered cost function to drive the optimization toward a reasonable minimum point.
- The theoretical estimation accuracy of the proposed identification methods is rigorously characterized. The approaches and the associated analysis are validated using extensive simulations and experiments.

With the above contributions, our study can enable easier availability of accurate Thevenin's models for advanced battery management ranging from charging control to SoC estimation and aging prognostics.

The rest of the paper is organized as follows. Section 2 reviews the Thevenin's model and sets up the parameter identification problem. Section 3 investigates the parameter identifiability and develops the identification approaches. Section 4 evaluates the efficacy of the proposed results through Monte Carlo simulations. Section 5 further presents validation based on experiments. Finally, some concluding remarks are gathered in Section 6.

2. Thevenin's Model

This section first introduces the Thevenin's model and then derives the voltage response under constant-current discharging. The formulation of the parameter identification problem then follows.

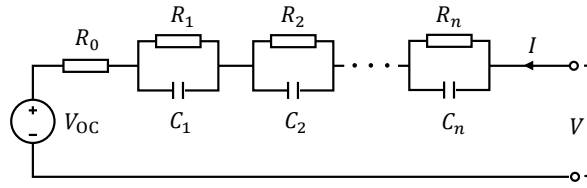


Figure 1: The Thevenin's equivalent circuit model.

A general form of the Thevenin's model is shown in Figure 1. The first main component of the model is a voltage source, which emulates a battery's OCV. The OCV is SoC-dependent, and the SoC's dynamics is given by

$$\text{SoC} = \frac{1}{3600Q_c} I, \quad (1)$$

where Q_c is the battery's maximum capacity in ampere-hour (Ah) and I is the current in ampere ($I < 0$ for discharging, and $I > 0$ for charging). The second component of this model, R_0 , represents the battery's internal resistance, which grasps the voltage drop in discharging and jump in charging. As the third component, a set of serially connected RC pairs can characterize the transient behavior in the battery's voltage response. This work considers only one RC pair, which is often sufficient practically and brings simplicity of analysis and computation. It is noteworthy that this will cause no loss of generality as the ensuing results can be extended to the case of multiple RC pairs.

By the Kirchoff's circuit laws, the voltage dynamics based on the one-RC Thevenin's model can be expressed as

$$\begin{cases} \dot{V}_{RC} = -\frac{1}{RC} V_{RC} - \frac{1}{C} I, \\ V = V_{OC} - V_{RC} + R_0 I, \end{cases} \quad (2a)$$

$$V = V_{OC} - V_{RC} + R_0 I, \quad (2b)$$

where V_{RC} is the voltage across the RC pair, V_{OC} the OCV, and V the terminal voltage. As aforementioned, V_{OC} is dependent on SoC. Following [16, 64], it can be characterized as a fifth-order polynomial with respect to SoC:

$$V_{OC}(\text{SoC}) = \sum_{i=0}^5 \alpha_i \text{SoC}^i, \quad (3)$$

where α_i for $i = 0, 1, \dots, 5$ are coefficients, and V_{OC} is lower and upper bounded, respectively, by $\underline{V}_{OC} = V_{OC}(\text{SoC} = 0)$ and $\overline{V}_{OC} = V_{OC}(\text{SoC} = 1)$. In addition, the literature often suggests the internal resistance R_0 as a function of SoC, which is in general constant but increases exponentially when SoC nears 0 [26, 65]. Hence, R_0 is parameterized as

$$R_0(\text{SoC}) = \beta_0 + \beta_1 e^{-\beta_2 \text{SoC}}, \quad (4)$$

where the coefficients $\beta_i > 0$ for $i = 0, 1, 2$.

From above, the Thevenin's model with one RC pair is represented by (1)-(4). Now, suppose that the battery is fully charged, left idling for a long period and then discharged by a constant current to cut-off voltage. Here, the focus on a constant-current discharging scenario for the sake of formulating a mathematically tractable identification problem. As another advantage, such a discharging protocol can be easily implemented in practice. Solving (2a) with $V_{RC}(t = 0) = 0$, one can obtain the evolution of V_{RC} under constant current through time as follows:

$$V_{RC}(t) = -IR \left(1 - e^{-\frac{t}{RC}}\right). \quad (5)$$

As a result, the terminal voltage V through time is

$$\begin{aligned} V(t) = & \alpha_0 + \alpha_1 \text{SoC}(t) + \alpha_2 \text{SoC}^2(t) + \alpha_3 \text{SoC}^3(t) + \alpha_4 \text{SoC}^4(t) + \alpha_5 \text{SoC}^5(t) \\ & + I\beta_0 + I\beta_1 e^{-\beta_2 \text{SoC}(t)} + IR \left(1 - e^{-\frac{t}{RC}}\right), \end{aligned} \quad (6)$$

where $\text{SoC}(t) = 1 + It/(3600Q_c)$ as indicated by (1), with $\text{SoC}(0) = 1$.

It is worth noting that \underline{V}_{OC} and \overline{V}_{OC} can be preset and used in the discharging experiments. It is also assumed that the total capacity Q_c is known or can be experimentally determined for given \underline{V}_{OC} and \overline{V}_{OC} . Because $\alpha_0 = \underline{V}_{OC}$ and $\sum_{i=0}^5 \alpha_i = \overline{V}_{OC}$, only α_i for $i = 1, 2, \dots, 4$ need to be determined. It is seen that (6) defines an explicit relationship between V , I and the unknown parameters, i.e., α_i for $i = 1, \dots, 4$, β_i for $i = 0, 1, 2$, R and C . The next problem to tackle is two-fold: 1) deciding if the parameters are identifiable, and 2) designing approaches to achieve effective parameter identification, which will be the focus of the next section. Note that the parameters are assumed to be constant throughout this paper in order to consider a representative and tractable problem.

3. Parameter Identification

Based on Section 2, this section aims to identify the unknown model parameters. It starts with investigating the parameter identifiability analysis, which shows that the parameters are locally identifiable and offers a method of determining the theoretical identification accuracy. Then, it synthesizes two identification methods, which are based on the notion of nonlinear least squares (NLS) but use constrained optimization and regularization, respectively, to address the non-convexity issue that arises in parameter estimation.

3.1. Identifiability Analysis

Consider (6), for which the unknown parameter vector is

$$\boldsymbol{\theta} = \left[\alpha_1 \quad \alpha_2 \quad \alpha_3 \quad \alpha_4 \quad \beta_0 \quad \beta_1 \quad \beta_2 \quad R \quad (RC)^{-1} \right]^\top.$$

Note that θ_i for $i = 1, 2, \dots, 9$ and its corresponding parameter will be used interchangeably in sequel. The terminal voltage V is measured at a sequence of sampling instants $\{t_k\}$ for $k = 1, 2, \dots, N$ with $t_1 = 0$. By (6), $V(t_k)$ can be compactly written as

$$V(t_k) = \phi(\boldsymbol{\theta}; t_k), \quad (7)$$

where

$$\begin{aligned} \phi(\boldsymbol{\theta}; t_k) = & \underline{V}_{OC} + \theta_1 \text{SoC}(t_k) + \theta_2 \text{SoC}^2(t_k) + \theta_3 \text{SoC}^3(t_k) + \theta_4 \text{SoC}^4(t_k) \\ & + \left(\bar{V}_{OC} - \underline{V}_{OC} - \sum_{i=1}^4 \theta_i \right) \text{SoC}^5(t_k) + \theta_5 I + \theta_6 I e^{-\theta_7 \text{SoC}(t_k)} + \theta_8 I (1 - e^{-\theta_9 t_k}). \end{aligned}$$

Given (7), a fundamental question is whether $\boldsymbol{\theta}$ can be uniquely identified from the data sequence $\{V(t_k)\}$, which boils down to the identifiability issue. To proceed, a definition of the local parameter identifiability is introduced for (7) as follows [49, 66].

Definition 1. A model structure $\phi(\boldsymbol{\theta}; t_k)$ is said to be locally identifiable at some point $\boldsymbol{\theta}^0$ in the parameter space for a given data sequence $\{V(t_1), V(t_2), \dots, V(t_N)\}$, if for any $\boldsymbol{\theta}^1$ and $\boldsymbol{\theta}^2$ within the neighborhood of $\boldsymbol{\theta}^0$, $\phi(\boldsymbol{\theta}^1; t_k) = \phi(\boldsymbol{\theta}^2; t_k)$ holds if and only if $\boldsymbol{\theta}^1 = \boldsymbol{\theta}^2$.

Definition 1 indicates that there should exist no two different parameter sets in the neighborhood of a point that can produce the same data sequence if the parameters are locally identifiable.

Before moving on to discuss the identifiability testing condition, let us consider the parameter identification problem for (7) in a prediction-error framework, seeking to find out the parameter estimates to minimize the difference between the measurements and the model-based predictions. To this end, an NLS cost function can be formulated as

$$J(\boldsymbol{\theta}) = \frac{1}{2} [\mathbf{y} - \boldsymbol{\phi}(\boldsymbol{\theta})]^\top \mathbf{Q}^{-1} [\mathbf{y} - \boldsymbol{\phi}(\boldsymbol{\theta})], \quad (8)$$

where \mathbf{Q} is a symmetric positive definite matrix interpretable as the covariance matrix of an additive measurement noise, and

$$\begin{aligned} \mathbf{y} &= \left[V(t_1) \quad V(t_2) \quad \dots \quad V(t_N) \right]^\top, \\ \boldsymbol{\phi}(\boldsymbol{\theta}) &= \left[\phi(\boldsymbol{\theta}; t_1) \quad \phi(\boldsymbol{\theta}; t_2) \quad \dots \quad \phi(\boldsymbol{\theta}; t_N) \right]^\top. \end{aligned}$$

The parameter estimation then lies in finding out $\hat{\theta}$ to minimize $J(\theta)$, i.e.,

$$\hat{\theta} = \arg \min_{\theta} J(\theta). \quad (9)$$

It is pointed out in [66] that evaluating the local identifiability of θ around $\hat{\theta}$ (see Definition 1) can be achieved by testing whether the minimization problem in (8) has a unique solution in the local parameter space. Further, a sufficient condition to guarantee a unique $\hat{\theta}$ (or in other words, the local identifiability of θ) is that the Hessian matrix $\partial^2 J(\theta)/\partial\theta^2 > \mathbf{0}$ at $\hat{\theta}$. To satisfy this condition, $\partial\phi(\theta)/\partial\theta$ at $\hat{\theta}$ must be of full rank. This is because the local first-order approximation of $\partial^2 J(\theta)/\partial\theta^2$ is

$$\frac{\partial^2 J(\theta)}{\partial\theta^2} \approx \left(\frac{\partial\phi(\theta)}{\partial\theta} \right)^\top \mathbf{Q}^{-1} \frac{\partial\phi(\theta)}{\partial\theta}.$$

Here, define $\mathbf{S}(\theta) = \partial\phi(\theta)/\partial\theta$. It is referred to as the sensitivity matrix and measures how the parameter perturbations can change the terminal voltage. The terminal voltage can be said to be sensitive to a parameter if it sees a relatively large change when the parameter varies slightly. A parameter with higher sensitivity generally allows for more accurate estimation. Meanwhile, $\mathbf{S}(\theta)$ should be of full rank as discussed above, so that when the parameters change, their effects on the terminal voltage are differentiable. Specifically, $\mathbf{S}(\theta)$ is given by

$$\mathbf{S}(\theta) = \begin{bmatrix} \vdots & \vdots & \vdots & \vdots \\ \frac{\partial\phi(\theta; t_k)}{\partial\theta_1} & \frac{\partial\phi(\theta; t_k)}{\partial\theta_2} & \dots & \frac{\partial\phi(\theta; t_k)}{\partial\theta_9} \\ \vdots & \vdots & \vdots & \vdots \end{bmatrix}_{N \times 9}, \quad (10)$$

where

$$\frac{\partial\phi(\theta; t_k)}{\partial\theta_i} = \text{SoC}^i(t_k) - \text{SoC}^5(t_k), \text{ for } i = 1, \dots, 4, \quad (11a)$$

$$\frac{\partial\phi(\theta; t_k)}{\partial\theta_5} = I, \quad (11b)$$

$$\frac{\partial\phi(\theta; t_k)}{\partial\theta_6} = I e^{-\theta_7 \text{SoC}(t_k)}, \quad (11c)$$

$$\frac{\partial\phi(\theta; t_k)}{\partial\theta_7} = -I \text{SoC}(t_k) \theta_6 e^{-\theta_7 \text{SoC}(t_k)}, \quad (11d)$$

$$\frac{\partial\phi(\theta; t_k)}{\partial\theta_8} = I (1 - e^{-\theta_8 t_k}), \quad (11e)$$

$$\frac{\partial\phi(\theta; t_k)}{\partial\theta_9} = I \theta_8 t_k e^{-\theta_8 t_k}, \quad (11f)$$

for $k = 1, 2, \dots, N$. From above one can observe that the columns of $\mathbf{S}(\theta)$ are linearly independent, making $\mathbf{S}(\theta)$ a full-rank matrix. This conclusion can be further verified by computationally evaluating $\mathbf{S}(\theta)$ around the nominal parameters of a battery model, with further discussion offered in Section 4. Hence, one can claim that the parameter vector θ is locally identifiable.

Further, suppose that $\hat{\theta}$ is successfully estimated and minimizes $J(\theta)$. The covariance of $\hat{\theta}$ in the Gaussian case then is given by

$$\text{Cov}(\hat{\theta}) = \text{E} \left(\left[\left. \frac{\partial^2 J(\theta)}{\partial \theta^2} \right|_{\theta} \right]^{-1} \right) \approx [\mathbf{S}^\top(\theta) \mathbf{Q}^{-1} \mathbf{S}(\theta)]^{-1}, \quad (12)$$

from which the variance of the estimate $\hat{\theta}_i$ for $i = 1, 2, \dots, 9$, is the i -th diagonal element of $\text{Cov}(\hat{\theta})$, i.e., $[\text{Cov}(\hat{\theta})]_{ii}$. Here, it should be noted that $[\text{Cov}(\hat{\theta})]_{ii}$ measures the estimation error if the estimation is unbiased and one can use (12) to calculate the theoretically possible parameter estimation accuracy.

3.2. Identification Methods

The foregoing discussion poses a basic parameter estimation problem as shown in (8)-(9). Although the parameters are locally identifiable, solving the problem is still a challenge due to two difficulties. The first one stems from the nonlinearity of the model, as is seen from the voltage equation (6). As the second and more challenging difficulty, the minimization problem in (9) is non-convex. Although a numerical optimization procedure, e.g., the Gauss-Newton method, can be deployed to tackle the nonlinearity issue, the non-convexity may still lead the parameter search to local minimum points that are unphysical or unreasonable. To ensure correct parameter estimation, this work introduces constrained optimization and regularization to improve the problem formulation by using prior knowledge about parameters.

3.2.1. Constrained Optimization

To prevent parameter search approaching physically meaningless local minima, one can constrain the search within a parameter space believably correct. Specifically, one can roughly determine the lower and upper bounds of some parameters, use them to set up a limited search space and run numerical optimization within this space. In practice, it is not difficult to determine the bounds of some parameters for the Thevenin's model, because some coarse-grained knowledge of a battery, e.g., internal impedance, can be obtained from both experience and some simple observation or analysis of the measurement data. A further discussion of extracting prior knowledge of parameters is provided in Section 5. With this idea, the identification problem in (9) is modified as a constrained optimization problem:

$$\hat{\theta} = \min_{\theta} J(\theta), \quad (13a)$$

$$\text{s.t. } \underline{\theta} \leq \theta \leq \bar{\theta}, \quad (13b)$$

where $\underline{\theta}$ and $\bar{\theta}$ are the lower and upper bounds for θ , respectively. It is noted that (13) represents a constrained NLS problem, which can be addressed by the trust region or line search algorithms. Here, a trust region method is considered, and a brief overview about it is taken from [67] and offered below for completeness.

Let us begin with the unconstrained case and consider (13) without the constraint (13b). Suppose there is a current guess of the solution $\hat{\theta}_k$, where k is the iteration step number. For the trust region method, it first constructs a function

ψ_k , referred to as “model function”, to approximate the actual objective function J around the current guess $\hat{\theta}_k$. The model function ψ_k is based on the Taylor-series expansion of J around $\hat{\theta}_k$ and defined as follows:

$$\psi_k(s_k) = J(\hat{\theta}_k) + \mathbf{g}_k^\top s_k + \frac{1}{2} s_k^\top \mathbf{B}_k s_k, \quad (14)$$

where s_k is a step to be determined, $\mathbf{g}_k = \nabla J(\hat{\theta}_k)$, and $\mathbf{B}_k = \nabla^2 J(\hat{\theta}_k)$. Then, minimizing the objective function J reduces to finding a minimizer of the model function $\psi_k(s_k)$. Since $\psi_k(s_k)$ can be a poor approximation of J when the step s_k is too large, the trust region method bounds the search for a minimizer of $\psi_k(s_k)$ within some region around $\hat{\theta}_k$. Hence, one needs to solve the following subproblem in order to find out the best candidate step s_k :

$$\min_{s_k} \psi_k(s_k) \quad \text{s.t.} \quad \|\mathbf{D}_k s_k\| \leq \Delta_k, \quad (15)$$

where \mathbf{D}_k is a scaling matrix, $\|\cdot\|$ is the Euclidean norm, and Δ_k is the so-called trust region radius. It is then interesting to see whether s_k can bring a large enough drop in $J(\theta)$ if added to $\hat{\theta}_k$. A worthy metric for this is

$$\rho_k = \frac{J(\hat{\theta}_k) - J(\hat{\theta}_k + s_k)}{\psi_k(0) - \psi_k(s_k)}, \quad (16)$$

where $J(\hat{\theta}_k) - J(\hat{\theta}_k + s_k)$ is the actual reduction in $J(\theta)$, and $\psi_k(0) - \psi_k(s_k)$ the anticipated reduction. If ρ_k is greater than a threshold, it is safe to increase the trust-region radius by letting $\hat{\theta}_{k+1} = \hat{\theta}_k + s_k$ and then continuing the search. Otherwise, the trust region should be reduced, and rerun (15) at the same iterate point $\hat{\theta}_k$.

In the case of (13b) applied as a constraint, there are different ways to cope with this. An approach offered in [67] defines a new subproblem, in which $\psi_k(s_k)$ is replaced by

$$\psi'_k(s_k) = J(\hat{\theta}_k) + \mathbf{g}_k^\top s_k + \frac{1}{2} s_k^\top (\mathbf{B}_k + \mathbf{C}_k) s_k,$$

where \mathbf{C}_k is a matrix that results from the constraint. Similar to (14), this subproblem is then iteratively implemented to search for the optimal parameter estimates. Summarizing the above, one can obtain the constrained NLS method for the Thevenin’s model identification, which is named as C-NLS.

3.2.2. Regularization

Tikhonov regularization offers another way to help overcome the non-convexity issue. It involves a pre-estimation of the parameters and uses the prior guess to regularize the original cost function. Here, the pre-estimation is expected to be close to the truth so that its presence will then drive the optimization to run in the vicinity of the true parameter

values. The regularization-based parameter estimation problem is expressed as follows:

$$\min_{\boldsymbol{\theta}} \bar{J}(\boldsymbol{\theta}) = J(\boldsymbol{\theta}) + \frac{1}{2} (\boldsymbol{\theta} - \boldsymbol{\theta}_0)^\top \mathbf{P}_0^{-1} (\boldsymbol{\theta} - \boldsymbol{\theta}_0), \quad (17)$$

where $\boldsymbol{\theta}_0$ represents the prior guess of $\boldsymbol{\theta}$, and \mathbf{P}_0 is a diagonal positive matrix acting as a quantification of the confidence in the quality of $\boldsymbol{\theta}_0$. This formulation in (17) can be interpreted from a Bayesian perspective, where $\boldsymbol{\theta}$ is assumed to be a Gaussian random vector following $\mathcal{N}(\boldsymbol{\theta}_0, \mathbf{P}_0)$. More information about this Bayesian-perspective interpretation can be found in Appendix. Here, the selection of $\boldsymbol{\theta}_0$ and \mathbf{P}_0 depends on some prior knowledge of a battery under consideration, and further discussion is given in Section 5. To address the problem in (17), one can also consider the trust region method introduced in Section 3.2.1. Thus far the regularization-based NLS method is obtained, which is named as R-NLS.

3.2.3. Comparison of C-NLS and R-NLS

Both the C-NLS and R-NLS methods are developed to accomplish the parameter estimation for the Thevenin's model. Sharing the objective of overcoming the non-convexity issue, they both require some advance knowledge of the parameters (i.e., the parameter bounds $\underline{\boldsymbol{\theta}}$ and $\bar{\boldsymbol{\theta}}$ for C-NLS and prior guess $\boldsymbol{\theta}_0$ and \mathbf{P}_0 for R-NLS). Our experience suggests that the advance knowledge does not have to be accurate—even a coarse inference can lead to satisfactory estimation accuracy. It also turns out that one can gather it in some convenient ways, with a further discussion to be offered in Section 5 along with the elaboration of experiments.

Meanwhile, there are several interesting differences between the two approaches. The first one lies in the computational efficiency. It is noteworthy that the R-NLS is usually computationally faster as it is based on unconstrained optimization. A second difference is concerned with the parameter estimation accuracy. Based on [68], the theoretical estimation error for both approaches can be quantified as $\text{tr}(\boldsymbol{\Sigma})$, where tr denotes trace and

$$\boldsymbol{\Sigma} = \mathbb{E} \left[(\hat{\boldsymbol{\theta}} - \boldsymbol{\theta})(\hat{\boldsymbol{\theta}} - \boldsymbol{\theta})^\top \right] = \text{Cov}(\hat{\boldsymbol{\theta}}) + (\mathbb{E}[\hat{\boldsymbol{\theta}}] - \boldsymbol{\theta})(\mathbb{E}[\hat{\boldsymbol{\theta}}] - \boldsymbol{\theta})^\top. \quad (18)$$

Here, one can approximately view $[\boldsymbol{\Sigma}]_{ii}$ as a squared error between $\hat{\theta}_i$ and θ_i , and the second term of the rightmost-hand side is due to the bias of $\mathbb{E}[\hat{\boldsymbol{\theta}}]$ from $\boldsymbol{\theta}$. For the C-NLS method, the bias term in (18) will reduce to zero if the bounds are ideally selected. In view of (12), its theoretical estimation accuracy then is given by

$$\text{tr}(\boldsymbol{\Sigma}) = \text{tr} \left(\left[\mathbf{S}^\top(\boldsymbol{\theta}) \mathbf{Q}^{-1} \mathbf{S}(\boldsymbol{\theta}) \right]^{-1} \right). \quad (19)$$

By contrast, the R-NLS method produces biased estimates as it pushes the estimates toward $\boldsymbol{\theta}_0$. It follows from (17) that

$$\mathbb{E}[\hat{\boldsymbol{\theta}}] = \boldsymbol{\theta} + \left(\mathbf{I} + \mathbf{P}_0 \mathbf{S}^\top(\boldsymbol{\theta}) \mathbf{Q}^{-1} \mathbf{S}(\boldsymbol{\theta}) \right)^{-1} (\boldsymbol{\theta} - \boldsymbol{\theta}_0).$$

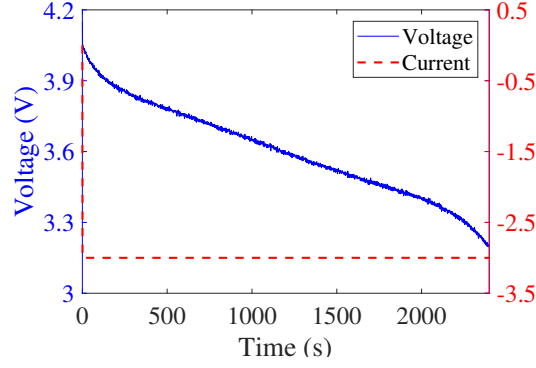


Figure 2: A model-based computer-generated terminal voltage profile for one Monte Carlo simulation.

This hence suggests that the theoretical estimation error of the R-NLS is

$$\text{tr}(\Sigma) = \text{tr} \left(\left[S^T(\theta) Q^{-1} S(\theta) + P_0^{-1} \right]^{-1} \right) + (\theta - \theta_0)^T \left(I + P_0 S^T(\theta) Q^{-1} S(\theta) \right)^{-T} \left(I + P_0 S^T(\theta) Q^{-1} S(\theta) \right)^{-1} (\theta - \theta_0). \quad (20)$$

Comparing (19) and (20), it is easy to notice the theoretical estimation accuracy attained by the two methods can be different, with the former being fixed and the latter dependent on θ_0 and P_0 . With distinct choices of θ_0 and P_0 , the R-NLS can be either more accurate than the C-NLS (e.g., $\theta_0 = \theta$ and $P_0 = \mathbf{0}$ as an extreme case) or less accurate (e.g., θ_0 is far away from θ and P_0 is close to $\mathbf{0}$). This indicates that one can leverage (20) as a guidance for the selection of θ_0 and P_0 , and a detailed discussion of this will be given in Section 4.

4. Monte Carlo Simulation

This section presents Monte Carlo simulation to verify the effectiveness of the C-NLS and R-NLS methods in extracting the Thevenin's model parameters. The simulation will further compare them in terms of estimation accuracy and computation time in accordance with the analysis in Section 3.2.3.

4.1. Training Data

The training data used in the Monte Carlo simulation are generated using the Thevenin's model with the following parameters: the nominal capacity $Q_c = 2.17$ Ah, $R = 0.0313$ Ω , $C = 1,858$ F, and

$$R_0(\text{SoC}) = 0.0313 + 0.0678 \cdot e^{-13.2 \cdot \text{SoC}},$$

$$V_{\text{OC}}(\text{SoC}) = 3.3 + 2.61 \cdot \text{SoC} - 9.36 \cdot \text{SoC}^2 + 19.7 \cdot \text{SoC}^3 - 19.0 \cdot \text{SoC}^4 + 6.9 \cdot \text{SoC}^5,$$

with $\underline{V}_{\text{OC}} = 3.3$ V and $\overline{V}_{\text{OC}} = 4.15$ V. Here, the battery parameters are drawn from the identification results on a Samsung INR18650-25R Li-ion battery used in Section 5.

Suppose the battery is discharged from full charge under a constant current I of -3 A by 2,400 s until when the terminal voltage reaches the cut-off voltage of 3.2 V. By (1), the SoC will decrease from 1 following

$$\text{SoC}(t) = 1 - \frac{1}{2604}t. \quad (21)$$

According to (6), the terminal voltage through time is given by

$$\begin{aligned} V(t) = & 3.3 + \theta_1 \cdot \text{SoC}(t) + \theta_2 \cdot \text{SoC}^2(t) + \theta_3 \cdot \text{SoC}^3(t) + \theta_4 \cdot \text{SoC}^4(t) \\ & + \left(4.15 - 3.3 - \sum_{i=1}^4 \theta_i \right) \cdot \text{SoC}^5(t) - \theta_5 \cdot 3 - \theta_6 \cdot 3e^{-\theta_7 \cdot \text{SoC}(t)} - \theta_8 \cdot 3(1 - e^{-\theta_9 t}), \end{aligned} \quad (22)$$

where θ_i for $i = 1, 2, \dots, 9$ make up the parameter vector $\boldsymbol{\theta}$ with

$$\boldsymbol{\theta} = \left[2.61 \quad -9.36 \quad 19.7 \quad -19.0 \quad 0.0313 \quad 0.0678 \quad 13.2 \quad 0.0313 \quad 0.0172 \right]^\top.$$

Let the terminal voltage $V(t)$ be sampled every second and corrupted by an additive white Gaussian noise with variance of 2.5×10^{-5} (i.e., $\boldsymbol{Q} = 2.5 \times 10^{-5} \boldsymbol{I}$ in (13) and (17)). Running (21)-(22), one can obtain an I - V dataset, with an example plotted in Figure 2. Further, repeat the same procedure for $M = 500$ times to create 500 datasets. These datasets, accounting for the effect of random noise sampling, can help develop statistically convincing conclusions about the performance of the proposed methods.

Before proceeding to parameter identification, one can first calculate the parameter sensitivity matrix $\boldsymbol{S}(\boldsymbol{\theta})$ based on the datasets to computationally verify the full rankness of $\boldsymbol{S}(\boldsymbol{\theta})$. It can be easily and consistently found out that $\boldsymbol{S}(\boldsymbol{\theta})$ is of full rank, showing that $\boldsymbol{\theta}$ is locally identifiable as previously analyzed.

4.2. Simulation Results

With the datasets generated and the parameters' local identifiability verified, let us now apply the C-NLS and R-NLS methods to each dataset for parameter estimation. Meanwhile, the original NLS problem (8) is also solved to provide a benchmark for comparison. Table 1 summarizes the initial guess for all the methods, $\underline{\boldsymbol{\theta}}$ and $\bar{\boldsymbol{\theta}}$ for the C-NLS, and $\boldsymbol{\theta}_0$ and \boldsymbol{P}_0 for the R-NLS. Note that the setting in Table 1 is coarse-grained relative to the truth. Here, consider the normalized root-mean-square error (NRMSE) to quantify the parameter estimation accuracy, which is defined as

$$\text{NRMSE}(\theta_i) = \sqrt{\frac{\frac{1}{M} \sum_{k=1}^M (\hat{\theta}_i[k] - \theta_i)^2}{\theta_i^2}}, \quad (23)$$

for $i = 1, 2, \dots, 9$. Recalling (19)-(20), one can notice that $\text{NRMSE}(\theta_i)$ is a sample-based computational estimation of $\sqrt{[\boldsymbol{\Sigma}]_{ii}/\theta_i^2}$. They are expected to be close if M is large enough.

Table 1: The simulation setting.

	Par	$\alpha_1/1$	$\alpha_2/1$	$\alpha_3/1$	$\alpha_4/1$	β_0/Ω	β_1/Ω	$\beta_2/1$	R/Ω	$(RC)^{-1}/s^{-1}$
	Initial Guess	1	1	1	1	0.029	0.4	40	0.2	1/40
C-NLS	θ	-	-	-	-	0.01	0	0	0	1/200
	$\bar{\theta}$	-	-	-	-	0.04	0.8	80	0.4	1
R-NLS	θ_0	1	1	1	1	0.029	0.4	40	0.2	1/40
	diag[\mathbf{P}_0]	50^2	50^2	50^2	50^2	0.001^2	0.1^2	10^2	0.06^2	0.005^2

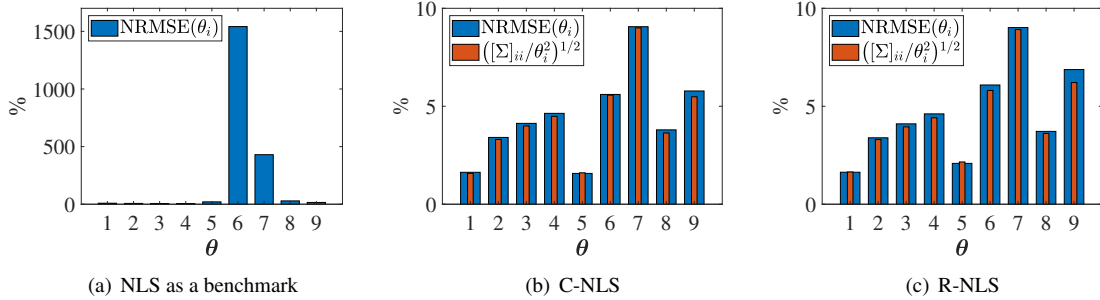


Figure 3: Parameter estimation errors for (a) NLS as a benchmark, (b) C-NLS and (c) R-NLS.

Figure 3 shows the NRMSE obtained by solving the original NLS problem (8) and applying the C-NLS and R-NLS methods, respectively. It is first seen that the NLS leads to extremely poor estimation accuracy, due to the intrinsic non-convexity as aforementioned. By comparison, both the C-NLS and R-NLS methods achieve substantial success, with the NRMSE lying below 10% for every parameter. Going deeper, let us look in more detail at θ_6 , i.e., the resistance β_1 . Figure 4 shows the histogram of the estimates of θ_6 produced by the three methods. As is seen, the NLS estimation constantly strays far away from the truth, but the C-NLS and R-NLS give estimates near the true value 0.0678 with considerable consistency. These observations suggest that the proposed methods are highly competent in identifying the Thevenin’s model parameters, even though the prior knowledge used is rough.

Taking a closer look at Figure 3, one can find out that the estimation errors calculated based on the Monte Carlo simulation results match well with the theoretical values. This validates the correctness of the theoretical analysis. In addition, an implication specific for the R-NLS is that one can make use of (20) to select θ_0 and \mathbf{P}_0 . To explore this implication, let us consider applying $\{\theta_0, \lambda \mathbf{P}_0\}$ with λ varying between 0 and 5 and $\{\theta_0, \mathbf{P}_0\}$ shown in Table 1. Figure 5 depicts the theoretical accuracy of the R-NLS with respect to λ , where var and bias correspond to the two terms in the rightmost-hand side of (20), respectively. Several observations can be drawn. First, λ plays a role in the estimation performance, or in other words, the selection of θ_0 and \mathbf{P}_0 will affect the eventual estimation accuracy. Second, the estimation accuracy will improve when λ increases and then keep at a same level after λ becomes large enough, and the nominal bias will approach zero. This indicates that the prior knowledge should be imposed with appropriate confidence and that it is wise to adopted a relatively large \mathbf{P}_0 if the prior knowledge is not precise. Finally, based on such a plot, a practitioner can choose θ_0 and \mathbf{P}_0 deemed as the best.

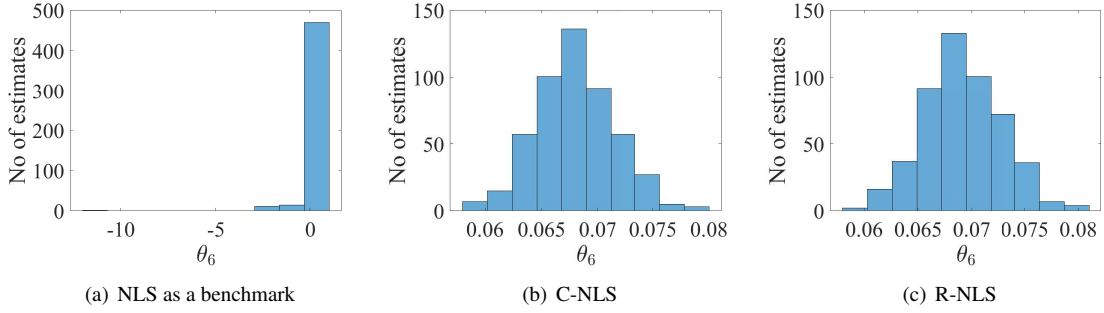


Figure 4: Histogram of estimates of θ_6 for (a) NLS as a benchmark, (b) C-NLS and (c) R-NLS.

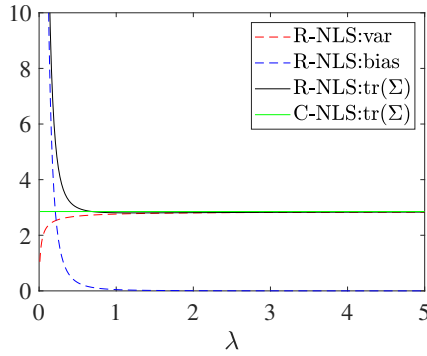


Figure 5: Theoretical estimation accuracy of the R-NLS method changes with λ .

Concluding this section is a comparison of the running time. All the simulations in this section are conducted on a Dell Precision Tower 3620 with 3 GHz Inter Xeon CPU and 16 Gb RAM running MATLAB R2018b. The computation time is averaged on the results of the 500 Monte Carlo runs. The original NLS, C-NLS and R-NLS on average take 88 ms, 142 ms, and 84 ms, respectively. From this result, one can find that both the C-NLS and R-NLS methods are computationally well affordable, especially given that they are designed for offline identification. Furthermore, the R-NLS computes faster, which comes as an additional advantage, because the regularization expedites the parameter search.

5. Experimental Validation

This section validates the C-NLS and R-NLS methods on experimental data. The experiments were conducted using a PEC[®] SBT4050 battery tester, which is shown in Figure 6. This tester has six channels and supports charging/discharging with arbitrary current-, voltage-, and power-based loads (up to 40 V and 50 A). It runs with a specialized server, which is used to configure a test offline and collect experimental data online, both through the associated software application LifeTestTM. The experiments were performed on a Samsung INR18650-25R Li-ion battery. One test was conducted first to generate the training data, from which the parameters are extracted. Then, three more



Figure 6: The experimental facility.

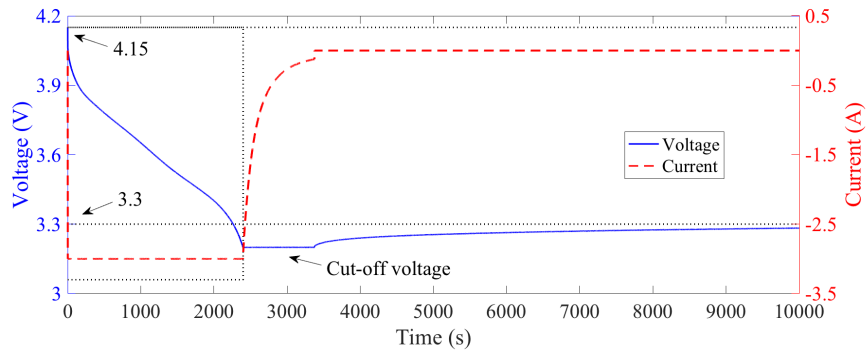


Figure 7: The voltage response of the Samsung INR18650-25R Li-ion battery in a constant-current/constant-voltage discharging experiment.

experiments were performed to generate validation datasets, to which the identified model is applied to assess its predictive performance.

5.1. Parameter Identification with Training Data

Considering $\underline{V}_{OC} = 3.3$ V and $\bar{V}_{OC} = 4.15$ V, the first experiment discharged the battery under room temperature using a constant current of -3 A from full charge until the terminal voltage hit the cut-off threshold of 3.2 V and then switched to constant-voltage discharging until the battery was fully depleted (when the current reduced to 0.125 A). The voltage asymptotically recovered to 3.3 V after the battery rested for a long time. Figure 7 shows the obtained current and voltage profiles. It should be noticed that a constant-voltage discharging phase was included here in order to determine the battery's total capacity. One can safely remove it if the capacity is known prior. Based on Figure 7, the battery's nominal capacity was calculated as $Q_c = 2.17$ Ah using coulomb counting [29]. Provided the I - V data in the constant-current discharging stage (encompassed by the black dotted-line box in Figure 7), the C-NLS and R-NLS methods were applied to extract parameter estimates, using the information setting in Table 1. Meanwhile, the original NLS problem (8) was also solved as a benchmark.

Before examining the parameter identification results, let us explain how the information in Table 1 is determined through the summary below. Here, the initial guess is used to initialize the identification run for all the methods; θ

and $\bar{\theta}$ are the parameter bounds for the C-NLS, and θ_0 and P_0 represent the advance knowledge used by the R-NLS.

- The parameters α_1 through α_4 are hard to guess in advance as they have no physical meaning, so they are simply initialized to be one. There is also no need to assign bounds for them in the C-NLS case. In the R-NLS case, it is safe to leave the elements of θ_0 and P_0 corresponding to them as blank, but if one wants to calculate the theoretical accuracy using (20), it is acceptable to set θ_0 without much care about accuracy and meanwhile set a large P_0 as in Table 1.
- The parameter β_0 is roughly equal to the immediate voltage drop upon the start of discharging divided by the applied current. From Figure 7, it is estimated as 0.029. Since this guess can be close to the truth, it is reasonable to stipulate a prior 99% confidence interval of 0.029 ± 0.003 for β_0 , where the standard deviation is 0.001, to run the R-NLS. For the execution of the C-NLS, the bounds are loosely set as 0.01 and 0.04.
- The voltage recovery after the end of the entire discharging process is largely due to the loss of voltage across $R_0(\text{SoC} = 0) = \beta_0 + \beta_1$. Hence, β_1 is upper bounded by $0.1/0.125 = 0.8$ based on Figure 7. Its lower bound is assigned to be zero for simplicity. The average of the bounds, 0.4, hence is chosen as the initial guess of β_1 , along with a standard deviation of $0.4/3$.
- The parameter β_2 mostly determines the curve shape of $R_0(\text{SoC})$. Its lower and upper bounds are very loosely set as 0 and 80. It is hence initially guessed as 40, which is the average of the bounds, with a standard deviation of $40/3$.
- The total voltage decline, following the immediate voltage drop when the discharging starts and lasting until when the constant-current discharging terminates, is from 4.15 V to 3.2 V. This is contributed by the combined change in the OCV and the voltage across R_0 and R . Note that the voltage across R will also approach a constant (i.e., IR) after sufficiently long time. The information can be used to infer an upper bound for R at 0.4 and a simple lower bound at 0. The average of the bounds, 0.2, is set as the initial guess, and the standard deviation set as $0.2/3$.
- Because RC is the time constant for the RC circuit, its value can be roughly seen from the voltage curve during the constant-current discharging. The voltage starts to decline almost linearly after the first 200 s, implying that RC is vaguely around $200/5 = 40$. The initial guess of $(RC)^{-1}$ is thus taken to be $1/40$, with a standard deviation of 0.005. Loose lower and upper bounds are chosen, which are $1/200$ and 1, respectively.

From above, one can develop some advance knowledge of the parameters through straightforward observation and analysis of the data and build an information setting as shown in Table 1. This allows the proposed C-NLS and R-NLS methods to easily lend themselves to use in practice.

With the above settings and letting $\mathbf{Q} = 2.5 \times 10^{-5} \mathbf{I}$, the original NLS, C-NLS and R-NLS are applied to estimate the parameters. The parameter estimates are summarized in Table 2, and the voltage data fitting shown in Figure 8.

Table 2: Parameter estimates for the battery used in the experiments.

Name	$\alpha_1/1$	$\alpha_2/1$	$\alpha_3/1$	$\alpha_4/1$	β_0/Ω	β_1/Ω	$\beta_2/1$	R/Ω	$(RC)^{-1}/s^{-1}$
$\hat{\theta}_{\text{Benchmark}}$	3.48	-11.3	20.5	-17.0	0.0360	0.0465	155	0.0668	0.0070
$\hat{\theta}_{\text{C-NLS}}$	2.61	-9.36	19.7	-19.0	0.0313	0.0678	13.2	0.0313	0.0172
$\hat{\theta}_{\text{R-NLS}}$	2.60	-9.34	19.7	-19.0	0.0308	0.0689	13.2	0.0313	0.0179

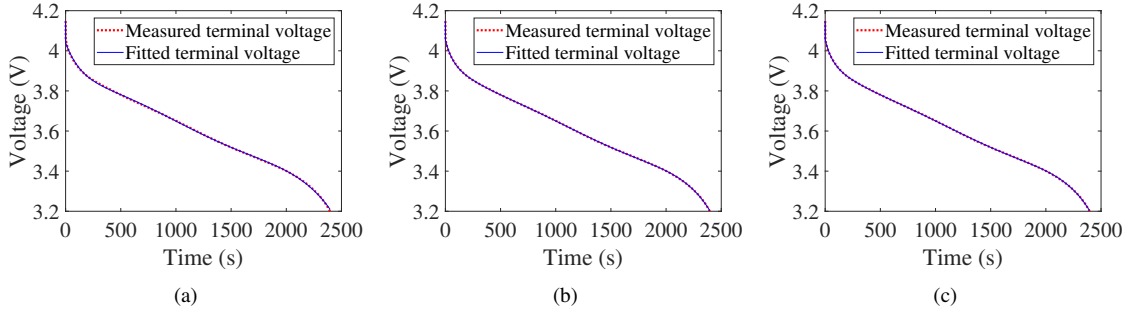


Figure 8: Comparison of measured and fitted terminal voltage for (a) NLS as a benchmark, (b) C-NLS and (c) R-NLS.

Figure 8 displays that the predicted terminal voltage well overlaps the measurements in all three cases. However, with a look at Table 2, it is interesting to find out that the C-NLS and R-NLS produce very close estimation, whereas the estimates of the original NLS are quite different. Next, validation data are utilized to further evaluate the quality of the three identified models.

5.2. Model Validation with Validation Data

Further experiments were conducted to generate datasets used to assess the performance of the above identified model. The first experiment, based on intermittent discharging, was designed to validate the accuracy of the estimated SoC-OCV relationships and impedance parameters. In this experiment, the battery was discharged by a constant current of -1 A for ten minutes and then left at rest for two hours such that the battery voltage would recover to a steady state. Such a procedure repeated itself until the voltage declined to the cut-off voltage of 3.2 V. The current and voltage profiles of this experiment are shown in Figure 9. This dataset allowed us to perform the following validation to verify the effectiveness of the proposed C-NLS and R-NLS methods.

- First, since the terminal voltage after a two-hour recovery can be regarded as the OCV, one can plot the SoC-OCV and use it as the ground truth to evaluate the estimated SoC-OCV relationship. Figure 10 offers such a comparison. Evidently, the SoC-OCV relationships identified by the C-NLS and R-NLS methods match well with the measured one. Contrasting this is a serious discrepancy in the benchmark case based on the original NLS.
- Second, the voltage recovery upon a pause of discharging can be largely attributed to the change in the voltage across R_0 and R , which is equal to $I(R_0 + R)$. Hence, $R_0 + R$ corresponding to different SoC levels can be

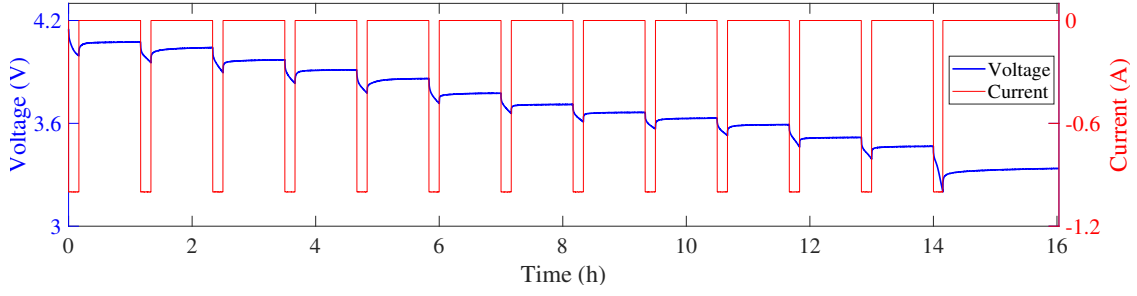


Figure 9: The voltage response of the battery in an intermittent discharging test.

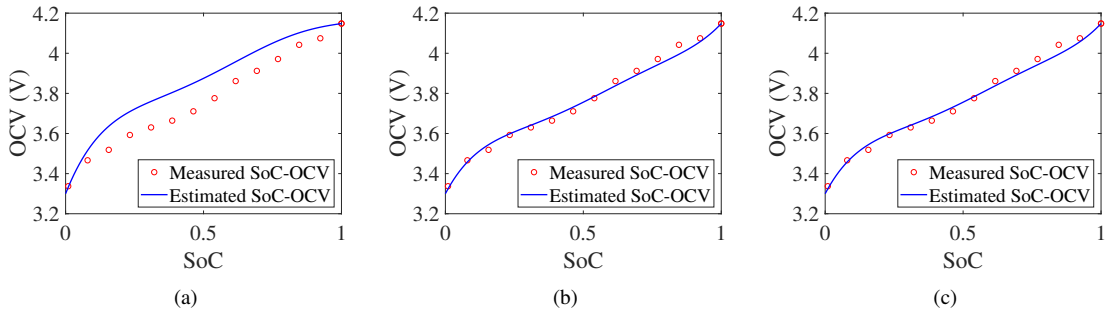


Figure 10: Comparison of measured and estimated SoC-OCV for (a) NLS as a benchmark, (b) C-NLS and (c) R-NLS.

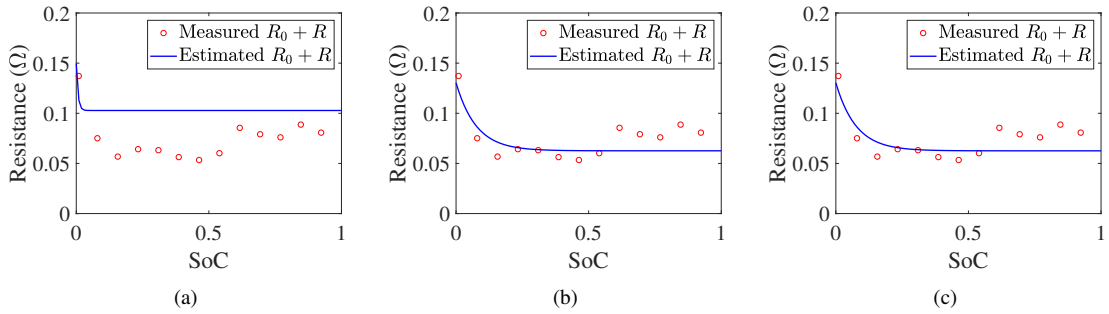


Figure 11: Comparison of measured and estimated $R_0 + R$ for (a) NLS as a benchmark, (b) C-NLS and (c) R-NLS.

determined and used to appraise the estimated values, as shown in Figure 11. The C-NLS and R-NLS are also observed to achieve more precise estimation than the original NLS in this case.

Another experiment applied a variable current profile to the battery, which was created based on the Urban Dynamometer Driving Schedule (UDDS) [69]. Figure 12 displays the UDDS-based current profile, which involves both charging and discharging in the run. Then, the identified models by the NLS, C-NLS and R-NLS methods are used to predict the terminal voltage under the current profile. Figure 13(a) compares the predicted voltage against the actual measurements. An overall excellent fitting accuracy can be observed for the models identified by the C-NLS and R-NLS, whereas for the benchmark NLS the accuracy is far from satisfactory. Figure 13(b) further plots the

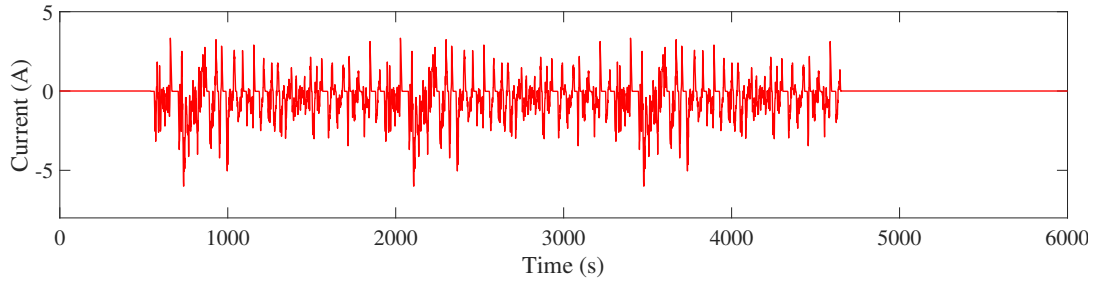


Figure 12: Variable currents from normalization of the Urban Dynamometer Driving Schedule (UDDS) profile.

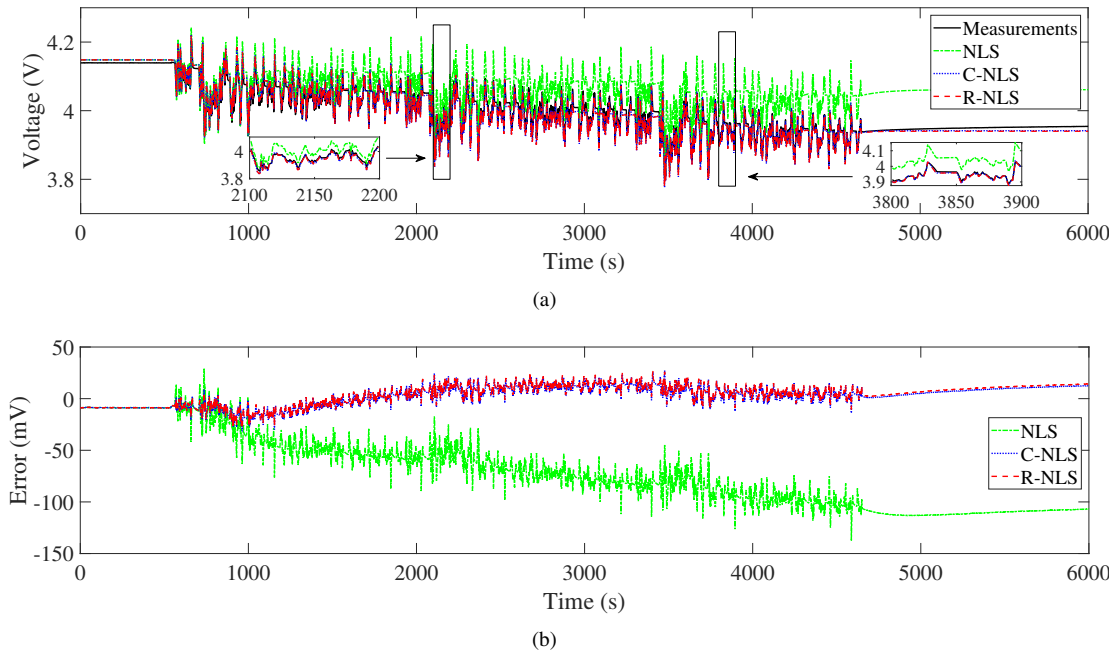


Figure 13: UDDS: (a) comparison of measured and estimated voltage for the benchmark NLS, C-NLS and R-NLS methods and (b) errors.

prediction errors, which are found to be generally less than 20 mV for the C-NLS and R-NLS and larger by a great margin for the original NLS. This validation provides clear-cut evidence that the identified models by the C-NLS and R-NLS are accurate, justifying the effectiveness and competence of the two methods for parameter identification. An experiment based on the Worldwide harmonized Light-duty vehicles Test Procedure (WLTP) [70] also shows similar results, though they are not reported here for the sake of space.

6. Conclusion

This paper studied the open problem of one-shot parameter identification for the popular Thevenin's battery model. The objective was to build an approach capable of estimating all model parameters offline from the current/voltage data in a single run. The study formulated the identification problem in a prediction-error-based framework and conducted the identifiability analysis, unveiling that the parameters of the Thevenin's model are locally identifiable.

Given the nonlinearity of the identification problem, numerical optimization was considered, but the non-convexity of the cost function inflicted local minimum trouble on the optimization procedure. This work then took two approaches to deal with this challenge, one imposing parameter bounds to constrain the search space, and the other regularizing the cost function with prior knowledge of the parameters. The resultant two identification methods, along with the identifiability analysis, were extensively validated through simulation and experiments. The proposed methods can provide high-quality parameter estimation and are relatively easy to implement with a one-shot run, having a potential for many battery management applications relying on accurate models, e.g., optimal charging, SoC estimation and monitoring of aging condition. Our future work will extend the investigation to the identification of Thevenin's models with temperature- and SoC-dependent parameters.

Appendix

The formulation in (17) can be interpreted from a Bayesian perspective [71]. Bayesian probabilistic estimation is concerned with determining the *a posteriori* distribution of θ given the measurements \mathbf{y} or $p(\theta|\mathbf{y})$, where $p(\cdot|\cdot)$ denotes conditional probability density function (pdf). According to the Bayes' rule, one has

$$p(\theta|\mathbf{y}) = \frac{p(\mathbf{y}|\theta)p(\theta)}{p(\mathbf{y})} \propto p(\mathbf{y}|\theta)p(\theta).$$

Consider that the measurement \mathbf{y} is corrupted by noise \mathbf{w} , as often happens in practice. That is,

$$\mathbf{y} = \phi(\theta) + \mathbf{w}.$$

If \mathbf{w} is independent of θ and follows a Gaussian distribution $\mathcal{N}(\mathbf{0}, \mathbf{Q})$, then $p(\mathbf{y}|\theta) \sim \mathcal{N}(\phi(\theta), \mathbf{Q})$. Meanwhile, θ is a Gaussian random vector. Its *a priori* pdf before the observation of \mathbf{y} is $p(\theta) \sim \mathcal{N}(\theta_0, \mathbf{P}_0)$. Then, it follows that

$$p(\theta|\mathbf{y}) \propto \exp\left(-\frac{1}{2}[\mathbf{y} - \phi(\theta)]^\top \mathbf{Q}^{-1}[\mathbf{y} - \phi(\theta)]\right) \exp\left(-\frac{1}{2}(\theta - \theta_0)^\top \mathbf{P}_0^{-1}(\theta - \theta_0)\right).$$

From the perspective of estimation, it is desired to find out θ to maximize $p(\theta|\mathbf{y})$. This is known as maximum a posteriori (MAP) estimation and can reduce to the problem shown in (17) by considering the log likelihood.

References

- [1] M. Coleman, C. K. Lee, C. Zhu, W. G. Hurley, State-of-charge determination from EMF voltage estimation: Using impedance, terminal voltage, and current for lead-acid and lithium-ion batteries, *IEEE Transactions on Industrial Electronics* 54 (5) (2007) 2550–2557.
- [2] S. Lee, J. Kim, J. Lee, B. Cho, State-of-charge and capacity estimation of lithium-ion battery using a new open-circuit voltage versus state-of-charge, *Journal of Power Sources* 185 (2) (2008) 1367–1373.
- [3] H. E. Perez, S. J. Moura, Sensitivity-based interval PDE observer for battery SOC estimation, in: 2015 American Control Conference, 2015, pp. 323–328.

- [4] Y. Wang, H. Fang, L. Zhou, T. Wada, Revisiting the state-of-charge estimation for lithium-ion batteries: A methodical investigation of the extended Kalman filter approach, *IEEE Control Systems* 37 (4) (2017) 73–96.
- [5] C.-C. Lin, H. Peng, J. W. Grizzle, J.-M. Kang, Power management strategy for a parallel hybrid electric truck, *IEEE Transactions on Control Systems Technology* 11 (6) (2003) 839–849.
- [6] H. Fang, Y. Wang, J. Chen, Health-aware and user-involved battery charging management for electric vehicles: Linear quadratic strategies, *IEEE Transactions on Control Systems Technology* 25 (3) (2017) 911–923.
- [7] H. Fang, C. Depcik, V. Lvovich, Optimal pulse-modulated lithium-ion battery charging: Algorithms and simulation, *Journal of Energy Storage* 15 (2018) 359–367.
- [8] H. E. Perez, X. Hu, S. Dey, S. J. Moura, Optimal charging of Li-ion batteries with coupled electro-thermal-aging dynamics, *IEEE Transactions on Vehicular Technology* 66 (9) (2017) 7761–7770.
- [9] J. Liu, G. Li, H. K. Fathy, An extended differential flatness approach for the health-conscious nonlinear model predictive control of lithium-ion batteries, *IEEE Transactions on Control Systems Technology* 25 (5) (2017) 1882–1889.
- [10] Q. Ouyang, J. Chen, J. Zheng, H. Fang, Optimal cell-to-cell balancing topology design for serially connected lithium-ion battery packs, *IEEE Transactions on Sustainable Energy* 9 (1) (2018) 350–360.
- [11] X. Lin, H. E. Perez, S. Mohan, J. B. Siegel, A. G. Stefanopoulou, Y. Ding, M. P. Castanier, A lumped-parameter electro-thermal model for cylindrical batteries, *Journal of Power Sources* 257 (2014) 1–11.
- [12] N. Tian, H. Fang, Y. Wang, 3-D temperature field reconstruction for a lithium-ion battery pack: A distributed Kalman filtering approach, *IEEE Transactions on Control Systems Technology* 27 (2) (2017) 847–854.
- [13] M. Dubarry, B. Y. Liaw, Development of a universal modeling tool for rechargeable lithium batteries, *Journal of Power Sources* 174 (2) (2007) 856–860.
- [14] B. Schweighofer, K. M. Raab, G. Brasseur, Modeling of high power automotive batteries by the use of an automated test system, *IEEE Transactions on Instrumentation and Measurement* 52 (4) (2003) 1087–1091.
- [15] G. L. Plett, Extended Kalman filtering for battery management systems of LiPB-based HEV battery packs: Part 2. Modeling and identification, *Journal of power sources* 134 (2) (2004) 262–276.
- [16] C. Weng, J. Sun, H. Peng, A unified open-circuit-voltage model of lithium-ion batteries for state-of-charge estimation and state-of-health monitoring, *Journal of Power Sources* 258 (2014) 228–237.
- [17] Y. Xing, W. He, M. Pecht, K. L. Tsui, State of charge estimation of lithium-ion batteries using the open-circuit voltage at various ambient temperatures, *Applied Energy* 113 (2014) 106–115.
- [18] H. He, R. Xiong, X. Zhang, F. Sun, J. Fan, State-of-charge estimation of the lithium-ion battery using an adaptive extended Kalman filter based on an improved Thevenin model, *IEEE Transactions on Vehicular Technology* 60 (4) (2011) 1461–1469.
- [19] Y. Tian, B. Xia, W. Sun, Z. Xu, W. Zheng, A modified model based state of charge estimation of power lithium-ion batteries using unscented Kalman filter, *Journal of Power Sources* 270 (2014) 619–626.
- [20] M. Petzl, M. A. Danzer, Advancements in OCV measurement and analysis for lithium-ion batteries, *IEEE Transactions on energy conversion* 28 (3) (2013) 675–681.
- [21] S. Abu-Sharkh, D. Doerffel, Rapid test and non-linear model characterisation of solid-state lithium-ion batteries, *Journal of Power Sources* 130 (1) (2004) 266–274.
- [22] S. Buller, M. Thele, E. Karden, R. W. De Doncker, Impedance-based non-linear dynamic battery modeling for automotive applications, *Journal of Power Sources* 113 (2) (2003) 422–430.
- [23] S. R. Nelatury, P. Singh, Equivalent circuit parameters of nickel/metal hydride batteries from sparse impedance measurements, *Journal of Power Sources* 132 (1) (2004) 309–314.
- [24] K. Goebel, B. Saha, A. Saxena, J. R. Celaya, J. P. Christophersen, Prognostics in battery health management, *IEEE Instrumentation & Measurement Magazine* 11 (4).
- [25] D. Andre, M. Meiler, K. Steiner, H. Walz, T. Soczka-Guth, D. Sauer, Characterization of high-power lithium-ion batteries by electrochemical

- impedance spectroscopy. II: Modelling, *Journal of Power Sources* 196 (12) (2011) 5349–5356.
- [26] M. Chen, G. A. Rincon-Mora, Accurate electrical battery model capable of predicting runtime and IV performance, *IEEE Transactions on Energy Conversion* 21 (2) (2006) 504–511.
- [27] J. Yang, B. Xia, Y. Shang, W. Huang, C. Mi, Improved battery parameter estimation method considering operating scenarios for HEV/EV applications, *Energies* 10 (1) (2016) 5.
- [28] F. Baronti, G. Fantechi, E. Leonardi, R. Roncella, R. Saletti, Enhanced model for lithium-polymer cells including temperature effects, in: *IECON 2010-36th Annual Conference on IEEE Industrial Electronics Society*, IEEE, 2010, pp. 2329–2333.
- [29] L. Lam, P. Bauer, E. Kelder, A practical circuit-based model for Li-ion battery cells in electric vehicle applications, in: *2011 IEEE 33rd International Telecommunications Energy Conference (INTELEC)*, IEEE, 2011, pp. 1–9.
- [30] A. Hentunen, T. Lehmuspelto, J. Suomela, Time-domain parameter extraction method for Thévenin-equivalent circuit battery models, *IEEE Transactions on Energy Conversion* 29 (3) (2014) 558–566.
- [31] D. Gandolfo, A. Brandão, D. Patiño, M. Molina, Dynamic model of lithium polymer battery-load resistor method for electric parameters identification, *Journal of the Energy Institute* 88 (4) (2015) 470–479.
- [32] M. Zheng, B. Qi, X. Du, Dynamic model for characteristics of Li-ion battery on electric vehicle, in: *2009 4th IEEE Conference on Industrial Electronics and Applications*, IEEE, 2009, pp. 2867–2871.
- [33] T. Kim, W. Qiao, A hybrid battery model capable of capturing dynamic circuit characteristics and nonlinear capacity effects, *IEEE Transactions on Energy Conversion* 26 (4) (2011) 1172–1180.
- [34] M. Einhorn, F. V. Conte, C. Kral, J. Fleig, Comparison, selection, and parameterization of electrical battery models for automotive applications, *IEEE Transactions on Power Electronics* 28 (3) (2012) 1429–1437.
- [35] C. Birkel, D. Howey, Model identification and parameter estimation for LiFePO₄ batteries, in: *Proceedings of IET Hybrid and Electric Vehicles Conference*, 2013, pp. 1–6.
- [36] J. Li, M. Mazzola, J. Gafford, N. Younan, A new parameter estimation algorithm for an electrical analogue battery model, in: *2012 Twenty-Seventh Annual IEEE Applied Power Electronics Conference and Exposition (APEC)*, IEEE, 2012, pp. 427–433.
- [37] X. Hu, S. Li, H. Peng, A comparative study of equivalent circuit models for Li-ion batteries, *Journal of Power Sources* 198 (2012) 359–367.
- [38] Z. Yu, L. Xiao, H. Li, X. Zhu, R. Huai, Model parameter identification for lithium batteries using the coevolutionary particle swarm optimization method, *IEEE Transactions on Industrial Electronics* 64 (7) (2017) 5690–5700.
- [39] H. Gu, Mathematical analysis of a Zn/NiOOH cell, *Journal of The Electrochemical Society* 130 (7) (1983) 1459–1464.
- [40] T. Hu, H. Jung, Simple algorithms for determining parameters of circuit models for charging/discharging batteries, *Journal of Power Sources* 233 (2013) 14–22.
- [41] L. Devarakonda, T. Hu, Algebraic method for parameter identification of circuit models for batteries under non-zero initial condition, *Journal of Power Sources* 268 (2014) 928–940.
- [42] X. Hu, L. Collins, S. Stanton, S. Jiang, A model parameter identification method for battery applications, Tech. rep., *SAE Technical Paper* (2013).
- [43] Y. Hu, S. Yurkovich, Linear parameter varying battery model identification using subspace methods, *Journal of Power Sources* 196 (5) (2011) 2913–2923.
- [44] Y. Li, C. Liao, L. Wang, L. Wang, D. Xu, Subspace-based modeling and parameter identification of lithium-ion batteries, *International Journal of Energy Research* 38 (8) (2014) 1024–1038.
- [45] B. Xia, X. Zhao, R. De Callafon, H. Garnier, T. Nguyen, C. Mi, Accurate lithium-ion battery parameter estimation with continuous-time system identification methods, *Applied Energy* 179 (2016) 426–436.
- [46] Y.-H. Chiang, W.-Y. Sean, J.-C. Ke, Online estimation of internal resistance and open-circuit voltage of lithium-ion batteries in electric vehicles, *Journal of Power Sources* 196 (8) (2011) 3921–3932.
- [47] M. Sitterly, L. Y. Wang, G. G. Yin, C. Wang, Enhanced identification of battery models for real-time battery management, *IEEE Transactions on Sustainable Energy* 2 (3) (2011) 300–308.

- [48] X. Tang, X. Mao, J. Lin, B. Koch, Li-ion battery parameter estimation for state of charge, in: American Control Conference (ACC), 2011, IEEE, 2011, pp. 941–946.
- [49] H. Fang, Y. Wang, Z. Sahinoglu, T. Wada, S. Hara, State of charge estimation for lithium-ion batteries: An adaptive approach, *Control Engineering Practice* 25 (2014) 45–54.
- [50] H. He, R. Xiong, H. Guo, Online estimation of model parameters and state-of-charge of LiFePO₄ batteries in electric vehicles, *Applied Energy* 89 (1) (2012) 413–420.
- [51] H. Rahimi-Eichi, F. Baronti, M.-Y. Chow, Online adaptive parameter identification and state-of-charge coestimation for lithium-polymer battery cells, *IEEE Transactions on Industrial Electronics* 61 (4) (2014) 2053–2061.
- [52] C. Fleischer, W. Waag, H.-M. Heyn, D. U. Sauer, On-line adaptive battery impedance parameter and state estimation considering physical principles in reduced order equivalent circuit battery models: Part 2. Parameter and state estimation, *Journal of Power Sources* 262 (2014) 457–482.
- [53] T. Feng, L. Yang, X. Zhao, H. Zhang, J. Qiang, Online identification of lithium-ion battery parameters based on an improved equivalent-circuit model and its implementation on battery state-of-power prediction, *Journal of Power Sources* 281 (2015) 192–203.
- [54] M. Ye, H. Guo, R. Xiong, Q. Yu, A double-scale and adaptive particle filter-based online parameter and state of charge estimation method for lithium-ion batteries, *Energy* 144 (2018) 789 – 799.
- [55] C. Zhang, W. Allafi, Q. Dinh, P. Ascencio, J. Marco, Online estimation of battery equivalent circuit model parameters and state of charge using decoupled least squares technique, *Energy* 142 (2018) 678 – 688.
- [56] Y. Hu, S. Yurkovich, Y. Guezennec, B. Yurkovich, A technique for dynamic battery model identification in automotive applications using linear parameter varying structures, *Control Engineering Practice* 17 (10) (2009) 1190–1201.
- [57] Y. Hu, S. Yurkovich, Y. Guezennec, B. Yurkovich, Electro-thermal battery model identification for automotive applications, *Journal of Power Sources* 196 (1) (2011) 449–457.
- [58] J. Brand, Z. Zhang, R. K. Agarwal, Extraction of battery parameters of the equivalent circuit model using a multi-objective genetic algorithm, *Journal of Power Sources* 247 (2014) 729–737.
- [59] A. Malik, Z. Zhang, R. K. Agarwal, Extraction of battery parameters using a multi-objective genetic algorithm with a non-linear circuit model, *Journal of Power Sources* 259 (2014) 76–86.
- [60] R. Rao, S. Vrudhula, D. N. Rakhmatov, Battery modeling for energy aware system design, *Computer* 36 (12) (2003) 77–87.
- [61] M. Jongerden, B. Haverkort, Battery modeling, Tech. rep., Centre for Telematics and Information Technology, University of Twente (2008).
- [62] G. L. Plett, *Battery Management Systems, Volume II: Equivalent-Circuit Methods*, Artech House, 2015.
- [63] A. Seaman, T.-S. Dao, J. McPhee, A survey of mathematics-based equivalent-circuit and electrochemical battery models for hybrid and electric vehicle simulation, *Journal of Power Sources* 256 (2014) 410–423.
- [64] A. Szumanowski, Y. Chang, Battery management system based on battery nonlinear dynamics modeling, *IEEE Transactions on Vehicular Technology* 57 (3) (2008) 1425–1432.
- [65] L. Lu, X. Han, J. Li, J. Hua, M. Ouyang, A review on the key issues for lithium-ion battery management in electric vehicles, *Journal of Power Sources* 226 (2013) 272–288.
- [66] J. F. Van Doren, S. G. Douma, P. M. Van den Hof, J. D. Jansen, O. H. Bosgra, Identifiability: from qualitative analysis to model structure approximation, *IFAC Proceedings Volumes* 42 (10) (2009) 664–669, 15th IFAC Symposium on System Identification.
- [67] T. F. Coleman, Y. Li, An interior trust region approach for nonlinear minimization subject to bounds, *SIAM Journal on Optimization* 6 (2) (1996) 418–445.
- [68] A. E. Hoerl, R. W. Kennard, Ridge regression: Biased estimation for nonorthogonal problems, *Technometrics* 12 (1) (1970) 55–67.
- [69] UDDS [Online], Available: <https://www.epa.gov/sites/production/files/2015-10/uddscol.txt>.
- [70] WLTP [Online], Available: <http://www.unece.org/fileadmin/DAM/trans/doc/2012/wp29grpe/WLTP-DHC-12-07e.xls>.
- [71] L. Ljung, T. Chen, What can regularization offer for estimation of dynamical systems?, *IFAC Proceedings Volumes* 46 (11) (2013) 1–8, 11th IFAC Workshop on Adaptation and Learning in Control and Signal Processing.